Experimental Investigation of Supercooled Water Droplet Breakup near the Leading Edge of an Airfoil

Belen Veras-Alba[1] and Jose Palacios[2]
The Pennsylvania State University, University Park, PA, 16802

Mario Vargas[3] and Charles Ruggeri[4]
NASA Glenn Research Center, Cleveland, OH, 44135

Tadas P. Bartkus[5]
Ohio Aerospace Institute, Cleveland, OH, 44135

This work presents the results of an experimental study on supercooled droplet deformation and breakup near the leading edge of an airfoil. The results are compared to prior room temperature droplet deformation results to explore the effects of droplet supercooling. The experiments were conducted in the Adverse Environment Rotor Test Stand (AERTS) at The Pennsylvania State University. An airfoil model placed at the end of the rotor blades mounted onto the hub in the AERTS chamber was moved at speeds ranging between 50 and 80 m/s. The temperature of the chamber was -20°C. A monotonic droplet generator was used to produce droplets that fell perpendicular to the airfoil path. High-speed imaging was employed to observe the interaction between the droplets and the airfoil. Cases with equal slip and initial velocity were selected for the two environmental conditions. The airfoil velocity was 60 m/s and the slip velocity for both sets of data was 40 m/s. The deformation of the weakly supercooled and warm droplets did not present different trends. The similar behavior for both conditions indicates that water supercooling has no effect on particle deformation for

---

[1] Graduate Student, Aerospace Engineering, 229 Hammond Building, AIAA Member
[2] Assistant Professor, Aerospace Engineering, 229 Hammond Building, AIAA Member
[3] Aerospace Engineer, Icing Branch, 21000 Brookpark Road, Associate Fellow AIAA
[4] Aerospace Engineer, Icing Branch, 21000 Brookpark Road, AIAA Member
[5] Senior Research Associate, Icing Branch, 21000 Brookpark Road, AIAA Member

the range of supercooling of the droplets tested and the selected impact velocity.

Nomenclature

$AERTS$ = Adverse Environment Rotor Test Stand

avi = Audio video interleave movie format

Bo = Bond number

D = Droplet diameter, μm

$DBKUP\ 002$ = Designation for airfoil used in experiment

f = Frequency, kHz

FAA = Federal Aviation Administration

$INTA$ = Instituto Nacional de Técnica Aeroespacial

LED = Light-emitting diode

μ = Dynamic viscosity, N s/m^2

$NACA$ = National Advisory Committee for Aeronautics

$NASA$ = National Aeronautics and Space Administration

PFV = Photron FASTCAM Viewer

Q = Flow rate, cm^3/min

Re = Reynolds number

ρ = Density, kg/m^3

σ = Surface tension, N/m

TAB = Taylor Analog Breakup

V_{slip} = Slip velocity, m/s

V = Velocity, m/s

We = Weber number

I. Introduction

AIRCRAFT manufacturers have reported in-flight observation of droplet breakup near the wing surfaces of large transport aircraft [1]. This observation is important for in-flight icing because if large droplets break up before impinging on aircraft surfaces, the smaller droplets that result may not impinge on the airfoil where predicted, potentially affecting the ice accretion process. If droplet breakup is a factor in the ice accretion process, current ice accretion codes will need to be modified to account for the breakup phenomena.

In 2005, the Federal Aviation Administration (FAA) sponsored a computational study by Wichita State University to assess the effects of aerodynamic forces on water droplets near the leading edge of an airfoil and the leading edges of the slat and flap elements of a high-lift airfoil [1]. Two-dimensional numerical computations of droplet breakup were done using the Taylor Analog Breakup (TAB) model in the commercial code FLUENT. The TAB model used included only vibrational and bag models of breakup. The effects of chord size and droplet diameter were studied for a NACA 0012 geometry for chords of 0.91 m (3 ft) and 6.1 m (20 ft) and droplet sizes of 100, 500, and 1000 micrometers. For the case of a 6.1-m (20-ft) chord airfoil, droplet breakup was studied for a three element airfoil high lift system in a landing configuration. The study indicated that droplets may break up in regions with severe pressure gradient. For the 0.91-m (3-ft) chord single element airfoil, the droplet breakup occurred aft of the leading edge. For the 6.1-m (20-ft) chord single element airfoil, the droplet breakup occurred near the stagnation region only. Large droplets were found to be more susceptible to breakup than smaller ones. They found that when droplet breakup occurred near the airfoil surface there was insufficient distance between the airfoil wall and the location where the droplet breakup was initiated for the droplets to achieve complete breakup before hitting the airfoil. The trajectory followed by droplets larger than 500 micrometers were "ballistic" in nature. The study pointed out the lack of experimental data in this area and recommended experimental tests to assess the effects on droplet breakup and breakup modes from the pressure gradient and the relative droplet-gas velocity near the leading edge of an airfoil.

In 2007, the National Aeronautics and Space Administration (NASA) Glenn Research Center and the Instituto Nacional de Técnica Aeroespacial (INTA) in Madrid, Spain, began an experimental

research program to obtain droplet breakup data on an airfoil configuration. A droplet breakup rotating rig was designed and built at the INTA installations near Madrid [2],[3]. The first sets of experiments were conducted at low speeds (15-66 m/s) in the fall of 2008. Using the experience gained from the low-speed experiments, the test rig was modified to attain speeds up to 90 m/s. Additional experiments were conducted between 2008 and 2012 for velocities from 50 to 90 meters per second and droplet sizes from 100 to 1800 micrometers [4]. The results allowed the gain of understanding on the phenomena and the behavior of the important parameters. The experiments were all conducted at room temperature. Since in in-flight icing the droplets are supercooled, the effect of supercooling was not answered at the time and remained an open research question.

The present work reports the results of a preliminary experiment conducted in the Adverse Environment Rotor Test Stand (AERTS) facility at The Pennsylvania State University to determine the effect of supercooling on droplet deformation and breakup as they approach the leading edge of an airfoil. In the AERTS facility, air temperatures below freezing can be reached and a range of droplet sizes can be supercooled. An airfoil model placed at the end of a rotating arm was moved at speeds between 50 and 80 m/s. A monosize droplet generator produced droplets from 200 to 700 micrometers that were allowed to fall from above, perpendicular to the path of the airfoil model at a given location. The temperature of the facility was maintained at -20 °C. The majority of the droplets were confirmed to be supercooled based on the measurement of the temperature of droplets at various distances from the exit of the droplet generator using an infrared camera and by using a temperature prediction code. The droplet temperature prediction code was used to verify the supercooling of the droplets based on the environmental conditions, water temperature at the droplet generator, the droplet size, and exit velocity. The prediction tool also confirmed the droplets could be supercooled at the impact location given the conditions provided. High-speed imaging was employed to observe the droplet deformation and breakup. A tracking software program was used to measure, from the high-speed movies, the droplet horizontal and vertical displacement against time. The horizontal displacement data was curve fitted to obtain the velocity and acceleration. The velocity and acceleration, together with experimental values of the air velocity at the locations of the droplet, were used to calculate the Bond, Weber, and Reynolds numbers along the path of the

droplet from beginning of deformation to breakup and/or hitting the airfoil. The parameter behavior and the droplet deformation were compared to results from studies done at room temperature.

In the present work, for the first time, droplet deformation and breakup experiments have been conducted using supercooled droplets approaching the leading edge of an airfoil. The possibility of SLD contributing to ridge ice accretions at the chordwise limit of ice protection systems along the span of lifting surfaces [5] and the work done at INTA with warm water droplets, which provided valuable information, point to the need for data using supercooled water droplets. The aim of the work presented is to provide data related to mildly supercooled water droplet deformation and breakup. While major differences were not expected due to the minor decrease in droplet temperature, the purpose was to compare the difference in the behavior of droplets above and below 0 °C. Although preliminary in nature given the complexity of the configuration, the results will help determine the validity of previous studies conducted at room temperature.

II. Experimental Setup

The experimental setup has four main elements: the rotor test stand, the airfoil mounted on the tip of the rotor blades, the monosize droplet generator, and the high-speed imaging system. In Figure 1, the conceptual view of the experiment setup with all of the elements except the high-speed imaging system and the illumination is shown. The experimental setup components in the test cell before a run is presented in Figure 2.

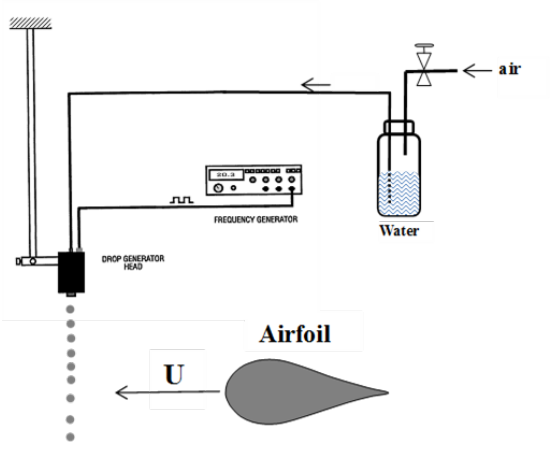

Fig. 1: Conceptual view of the experiment [4].

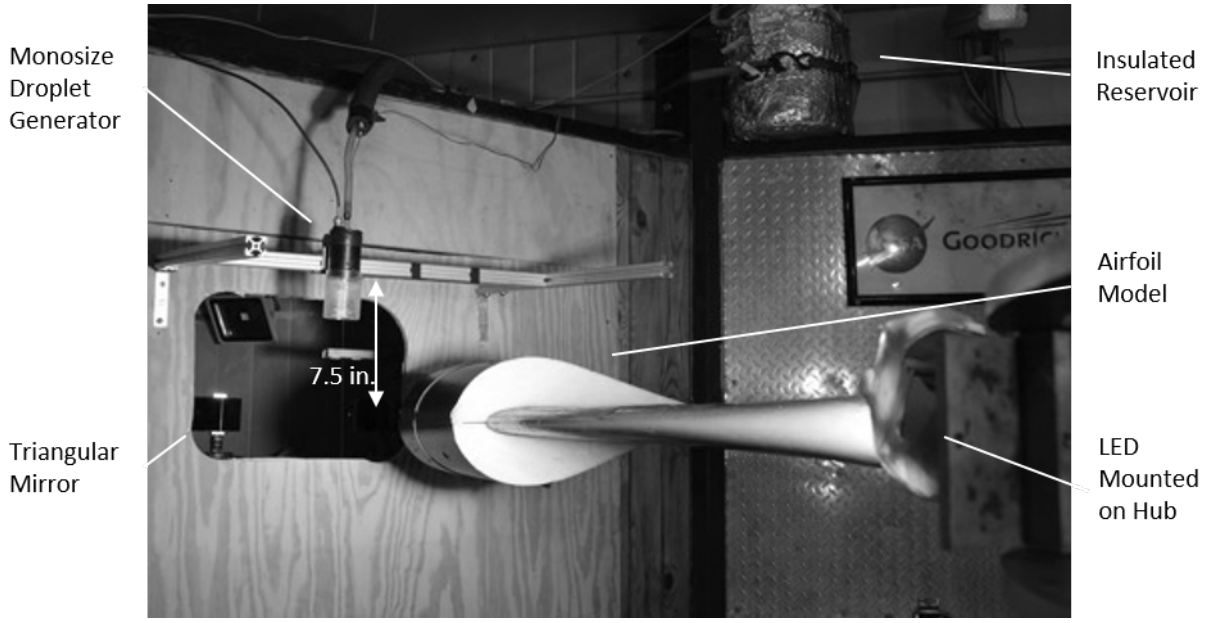

Fig. 2: Experimental setup in AERTS facility.

A. Adverse Environment Rotor Test Stand (AERTS)

The Adverse Environment Rotor Test Stand (AERTS) facility is located at Penn State University [6]. The facility was designed and is used to test and evaluate rotor blade ice protection systems. The AERTS facility is also used for ice protection coating evaluation and experimental rotor ice accretion shape correlation to ice shape modeling techniques. The facility is formed by an industrial 6 m x 6 m x 4 m (20 ft x 20 ft x 13 ft) cold chamber where temperatures between -25 °C and 0 °C (-13 °F to 32 °F) can be achieved [7]. The chamber is cooled by convection using cooling lines and a set of fans located inside the chamber. Inside the chamber and surrounding the rotor there is a ballistic wall in the shape of an octagon. The ballistic wall is formed by 15.2-cm (6-in) thick weather resistant lumber reinforced with 0.635 cm (0.25 in) thick steel and covered by aluminum plating for weather protection. A 93.2 kilowatt (125 hp) motor rotates the hub and the rotor. The chamber and its main components as seen from above are shown in Figure 3.

For the droplet breakup experiment, the AERTS facility was modified to accommodate the high-speed cameras for visualization of droplet deformation and impact with the airfoil. The imaging system was located behind one side of the ballistic wall. An opening in the ballistic wall allowed the cameras to observe and capture the droplet deformation events. A white 9500 lumens High Power LED from Cree was used for illumination. The LED was mounted on the hub of the rotor

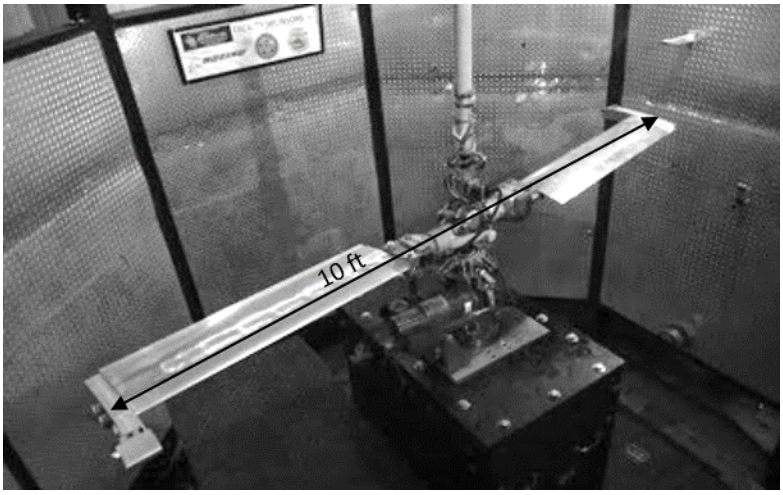

Fig. 3: Adverse Environment Rotor Test Stand.

(Figure 4). The airfoils were located at the tip of the rotor blades. The rotor blades were truncated QH-50 fiberglass blades. The radius of the rotor was 1.57 m (62 in). During the experiment, the rotor operated from 0 to 501 revolutions per minute. At the higher rotational speed, the airfoil was traveling at 80 m/s.

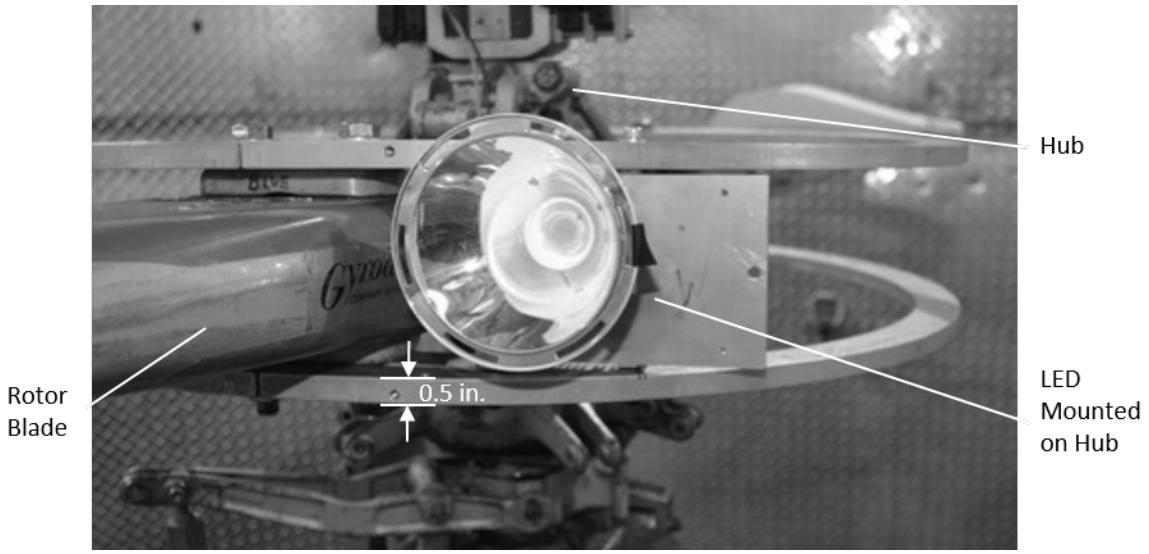

Fig. 4: LED mounted on hub.

B. Airfoil Model

The airfoil model mounted at the end of the rotor blades is a generic type of thick airfoil designated as DBKUP 002 (Figure 5). The airfoil was chosen for the experiment because it has a blunt shape geometry that simulates a scaled version of the type of leading edge shape found on

large transport airfoils. The airfoil measures 0.305 m (12 in) in the spanwise direction and has a chord length of 0.47 m (18.5 in).

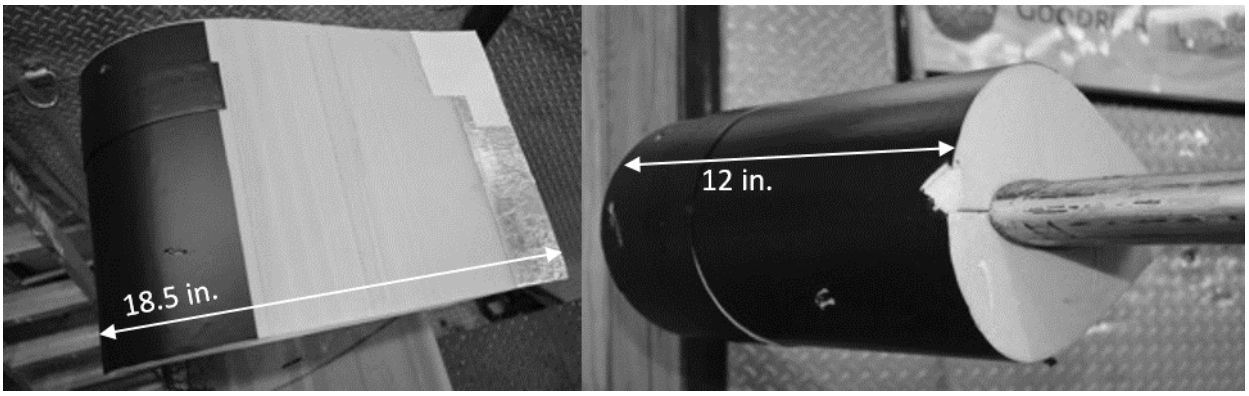

Fig. 5: DBKUP 002 airfoil model mounted on QH-50 rotor blade.

C. Monosize Droplet Generator

A TSI MDG-100 Monosize Droplet Generator was used to produce water droplets with an orifice diameter range from 100 μm to 500 μm. The droplet generator (Figure 6) was part of a system containing a pressurized water reservoir, a pressure controller, a frequency generator, and the vibration head. Air from a compressor pressurized the container and generated the water flow

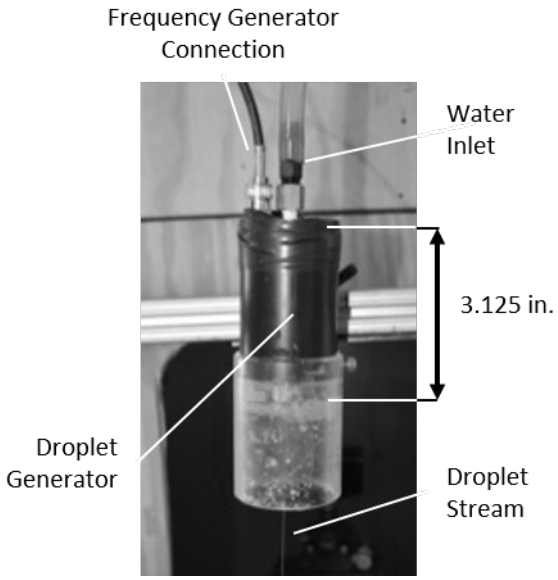

Fig. 6: TSI MDG-100 Monosize Droplet Generator.

from the tank to the vibration head – the small reservoir directly above droplet generator tip that

is vibrated at a specified frequency to break up the stream of water (see Figure 12). A pressure controller allowed for fine adjustment of the flow rate before the water reached the vibration head. At the vibration head, the water was forced through a small orifice and a jet was formed. A disturbance in the form of a square wave at the appropriate frequency was introduced by activating a piezoelectric transducer controlled with a BK Precision model 4011A frequency generator. The jet is unstable at resonant frequencies and breaks into uniform droplets. For a given orifice diameter, flow rate, and excitation frequency the diameter of the droplets generated is given by Equation 1:

$$D(\mu m) = \left[\frac{Q_{(}cc/min)}{f_{(}kHz)}\right]^{\frac{1}{3}} \tag{1}$$

where Q is the water flow rate in cubic centimeters per minute; f is the frequency in kilohertz; and D is the diameter of the droplets in micrometers. During the experiment, orifices of 200 and 400 μm were used. The pressurized container was a 5 gallon bucket with an airtight lid. The reservoir was insulated and modified to accommodate a bendable immersion heater as well as the 3.18 mm (0.125 in) OD air hose and tubing for the 12.7 mm (0.5 in) OD, 6.35 mm (0.25 in) ID water hose. The immersion heater was controlled by a PID controller to power it on and off as necessary to maintain the desired water reservoir temperature.

D. High-Speed Imaging System

The high-speed imaging system consisted of two high-speed cameras, the camera software, a triangular mirror and the lens system (Figure 7). The high-speed cameras used during the experiment were Photron SA-Z cameras. The cameras can capture images at rates from 1,000 to 1,000,000 frames per second (fps). During the experiment a frame rate of 90,000 fps was used. A resolution of 384Hx464V pixels was used. The dimensions of the field of view were 11.45 mm in the horizontal direction by 13.83 mm in the vertical direction. It corresponded to a resolution of 29.8 micrometers per pixel. The camera software employed for capturing the high-speed image sequences was Photron FASTCAM Viewer (PFV) and is part of the camera system. The same software was used for post-processing the image sequences to generate the data movies for data analysis. During

the experiment one lens configuration on each camera was used for magnification of the droplet deformation and/or breakup. The lens configuration consisted of a 200 mm Micro Nikkor lens with a 2x doubler added between the camera and the 200 mm lens to double the focal length of the microlens. Both cameras were placed 0.3 m (11.88 in) from the mirror. The distance from the tip of the mirror to the focal plane on the airfoil was 0.7 m (27.63 in) (Figure 8). The lighting was designed to illuminate the droplets from behind to create a shadowgraph (black color of the droplets against a white-gray background). The light source was a white 9500 lumens High Power LED from Cree mounted on a ring that was bolted to the blade grips.

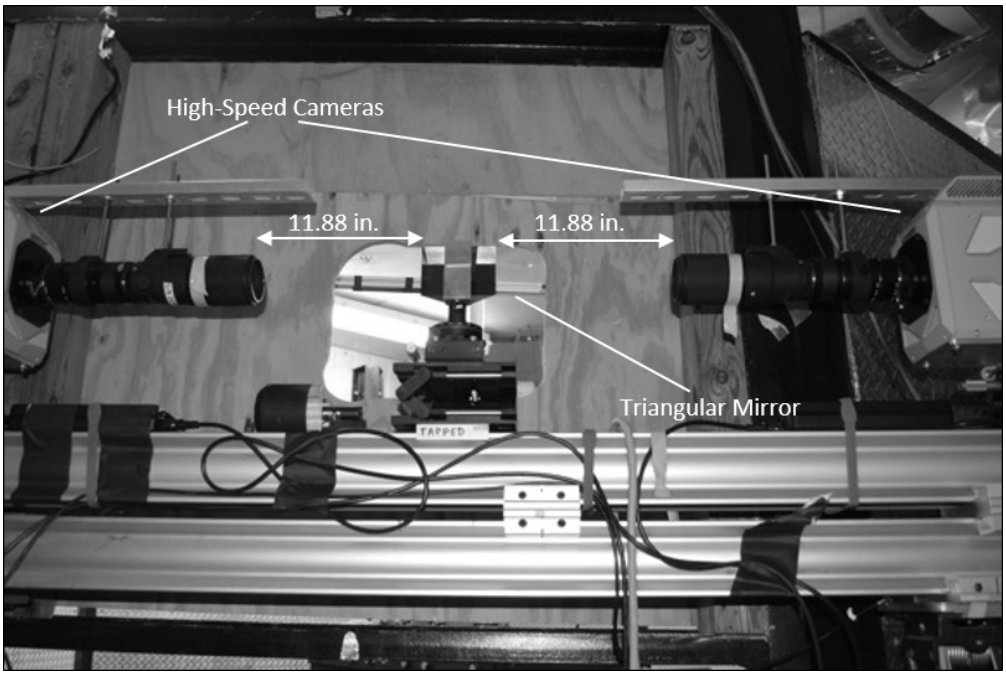

Fig. 7: Camera, lens, and triangular mirror setup.

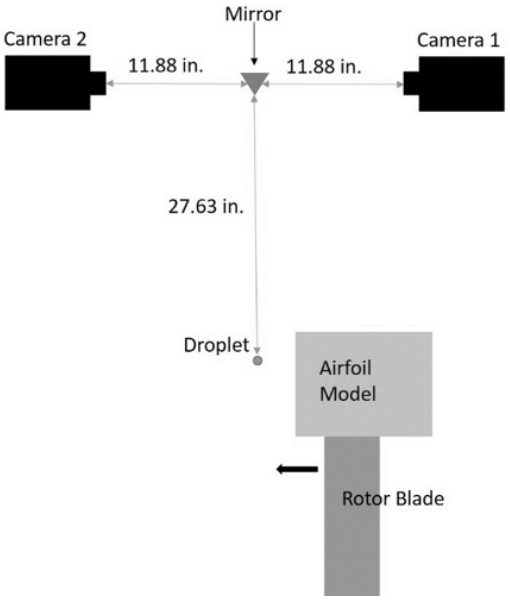

Fig. 8: Schematic of top view of camera and triangular mirror placement relative to airfoil model.

III. Test Procedure and Test Matrix

A. Test Procedure

Before a set of test runs, the high-speed cameras were aligned so that the line of view of the lens of each camera was parallel with the direction along the span of the airfoil at the midpoint of the leading edge (stagnation line along the span). The rotor blade was set at the position where the falling droplets from the monosize droplet generator just touched the leading edge. The airfoil was held at the same location during the alignment process. The cameras were placed, with respect to the triangular mirror, at the distance required by the optics to obtain the needed magnification and such that the center of the lens depth of field was at the location where the falling droplets grazed the airfoil leading edge. The motion of the cameras could carefully be controlled because each camera sat on a steel beam and on an x-y positioning table.

The airfoil was moved from the alignment position and a ruler with the smallest subdivision of one millimeter was placed at the location where the droplets grazed the leading edge of the airfoil. The camera was focused on the ruler and the number of pixels per millimeter was recorded. This conversion was used during the data analysis to measure the droplet diameter since the number of pixels in the camera sensor and the field of view are known.

The monosize droplet generator controls were adjusted to produce the range of droplet sizes

needed. The pressure and the frequency values were read from the calibration table obtained during the previous calibration of the system for the orifice being used in the generator. The pressure controller and the frequency generator were set at the corresponding values and the generator was started.

The personnel moved into the control room where they were able to observe the motion and operation of the rotor through different cameras positioned throughout the chamber. The cameras used for the experiments were controlled with software run on a laptop computer located in the control room. The software was used to start the cameras and set the controlling parameters including the frame rate and the shutter speed. The software allowed for writing of information that was part of the camera frames. It was located on each frame above the recorded image. This information was helpful during the data analysis. During the experiment, the following information was recorded on each frame: frame rate, time of recording, image resolution, frame number, lens configuration, date and time, airfoil velocity, and target droplet size.

The airfoilmodels were set in motion at the revolutions per minute corresponding to the target velocity. When it reached the target speed, the camera recording was started and maintained for several rotations. Once the recording was completed the rotor was brought to a stop. The high-speed movie was analyzed with the camera software to determine the quality of the recording of each of the passes of the airfoil. If the recording was deemed of good quality, the experiment moved to the next test point and the process was repeated.

B. Test Matrix

The test matrix for the experiment is shown in Table 1. The test matrix was designed to obtain data for rotor tip speeds of 50, 60, 70, and 80 m/s and for droplet generator orifice sizes of 200 and 400 μm. The pressure in the reservoir and the frequency of the piezoelectric transducer were varied to obtain the desired droplet sizes when using the different orifices. The higher frame rates of 150000 and 140000 fps were used initially and compared to the lower frame rate of 90000 fps to determine the widest view available with a resolution that allowed for observation of the droplet from no deformation to deformation and/or breakup. The chamber temperature was maintained

Table 1: Test matrix.

Date (2017)	Run	Orifice Size (μm)	FPS	Pressure (bar)	Frequency (kHz)	Resistance (kΩ)	Tw (°C)	Tc (°C)	RPM	Velocity (m/s)
2/21	1	200	140000	1.00	14.00	-	17.90	-	376	60.01
2/21	2	200	140000	0.91	14.00	-	15.90	-	376	60.01
2/21	3	200	140000	0.89	14.00	-	17.20	-	439	70.06
2/21	4	400	90000	0.89	50.00	-	17.30	-	314	50.11
2/21	5	400	90000	0.90	50.00	-	17.30	-	376	60.01
2/21	6	400	90000	0.90	50.00	-	17.20	-	376	60.01
2/21	7	400	90000	0.90	50.00	-	17.20	-	439	70.06
2/21	8	400	90000	0.90	50.00	-	17.20	-	439	70.06
2/21	9	400	150000	0.89	5.00	-	17.20	-	439	70.06
2/21	10	400	140000	0.89	5.00	-	17.20	-	439	70.06
2/22	1	400	90000	1.18	5.00	-	2.50	-20.0	313	49.95
2/22	2	400	90000	1.18	5.00	-	2.00	-20.0	313	49.95
2/22	3	400	90000	1.18	5.00	-	2.00	-22.6	313	49.95
2/22	4	400	90000	1.17	5.00	-	2.00	-22.7	376	60.01
2/22	5	400	90000	1.17	5.00	-	1.40	-22.7	376	60.01
2/23	1	200	90000	1.04	20.00	-	6.20	-17.2	314	50.11
2/23	2	200	90000	1.21	20.00	-	1.60	-21.4	314	50.11
2/23	3	200	90000	1.01	20.00	-	1.90	-14.0	376	60.01
2/23	4	200	90000	1.01	20.00	-	1.20	-14.0	376	60.01
2/24	1	200	90000	1.17	20.00	5.40	2.25	-24.6	314	50.11
2/24	2	200	90000	1.16	20.00	5.16	3.22	-21.0	376	60.01
2/24	3	200	90000	1.16	20.00	5.28	2.73	-21.2	439	70.06
2/24	4	200	90000	1.16	20.00	5.30	2.65	-20.4	439	70.06
2/24	5	200	90000	1.16	20.00	4.95	4.12	-19.6	501	79.96
2/24	6	200	90000	1.14	20.00	5.16	3.22	-19.0	500	79.80
2/24	7	200	90000	1.14	20.00	5.16	3.22	-18.9	500	79.80

above freezing while adjusting the cameras to establish the testing setup. Once the cameras were ready to begin testing, the chamber temperature was decreased to create the environment that would allow the droplets to supercool at the impact location. Initially, the temperature of the water was recorded only at the inlet to the droplet generator using a thermocouple. On the last day of testing, the temperature was collected at the inlet to the droplet generator using a thermistor while the thermocouple provided the temperature of the water near the reservoir.

IV. Droplet Supercooling Investigation

Prior to collecting the high-speed video in each test, the temperature of the water was recorded as it exited the reservoir and as it entered the droplet generator. A Type T thermocouple was inserted into the flow at the exit of the reservoir and used with a PID controller connected to the immersed water heater to maintain the water at a constant desired temperature. The water in the reservoir needed to be maintained around 9 °C to avoid freezing in the water hose and the droplet generator. A thermistor was inserted into the flow at the input of the droplet generator to measure the water temperature as close as possible to the droplet jetting location. During the tests, the temperature of the water, after the droplets exited the generator, was not recorded to avoid interfering with the airfoil models.

After the location of the droplet generator used in the experiments was established, the setup was repeated without spinning the rotor to measure the temperature of the water at four vertical distances from the tip of the droplet generator. The temperature of the water was recorded at 2.54, 7.62, 12.7, and 19.05 cm (1, 3, 5, and 7.5 in) below the droplet generator using an infrared (IR) camera and a black surface. The impact of the water droplets against the airfoil occurred at 19.05 cm (7.5 in) below the jetting location. A 200 μm orifice (with a flow rate of about 32.4 cc/min) was used and the droplets fell at a velocity approximately between 3 and 4 m/s. The resolution of the IR camera could not capture the droplets or stream to give a temperature reading. Therefore, a black plastic surface, which was at the chamber temperature of -20 °C, was used to allow the stream to impact on it allowing the IR camera to provide a temperature reading of the impacting water. An image taken with the IR camera along with a schematic of the setup is shown in Figure 9. The value of the maximum temperature seen in the top left corner shows the maximum temperature of the rectangle in the center of the image, it does not include the accumulation of water on the plastic surface. The range of temperatures in the entire image is shown by the scale on the right side of the thermal image and it ranges between -26.8 and -7.2 °C. It is expected that the temperature of the water will be the warmest in the image since all other objects were allowed to reach the chamber temperature.

The surface was provided by a black plastic case with a wall thickness of 0.32 cm (0.125 in),

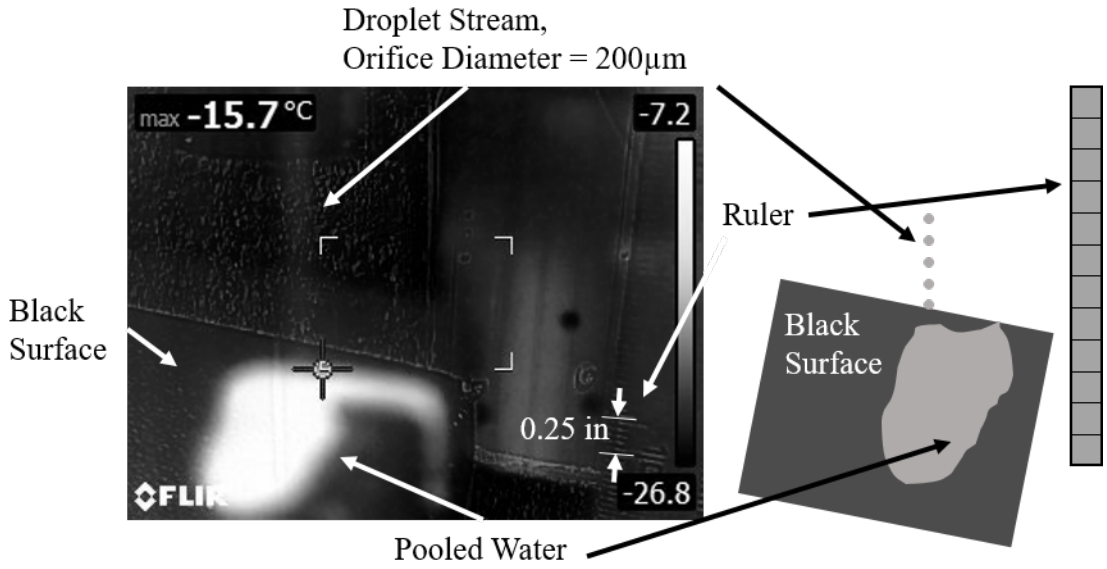

Fig. 9: Schematic and thermal image taken during the measurment of water temperature with infrared camera.

length of 30.48 cm (12 in), width of 10.8 cm (4.25 in), and height of 2.86 cm (1.125 in). The measurement approach estimated the temperature of the water droplets, but the black surface was at the environmental temperature (-20 °C) which has thermal energy that is expected to affect the measured water temperature. The mentioned shortcomings related to the measurement of the water droplet temperature using an infrared camera limits the validity of the data recorded. Such shortcomings are apparent by the large standard deviation observed on the experimental data and the unexplained increase in droplet temperature at the 19.05 cm (7.5 in) location (Figure 10). Presented in Figure 10 are the results of the experimental method used for measuring the droplet temperature at various vertical distances from the tip of the droplet generator. The experimental data suggests that the temperature of the water is below freezing at each point below the tip (exit) of the droplet generator.

For this reason, a prediction code by Tadas P. Bartkus, a NASA Glenn Research Center contractor, was used to give further confidence that the droplets were indeed supercooled [8]. A conservative approach was taken to predict the temperature of the water at the four distances below the tip of the droplet generator. This approach assumed that only convective cooling occurred between the location where the water temperature was measured above the droplet generator and the impact

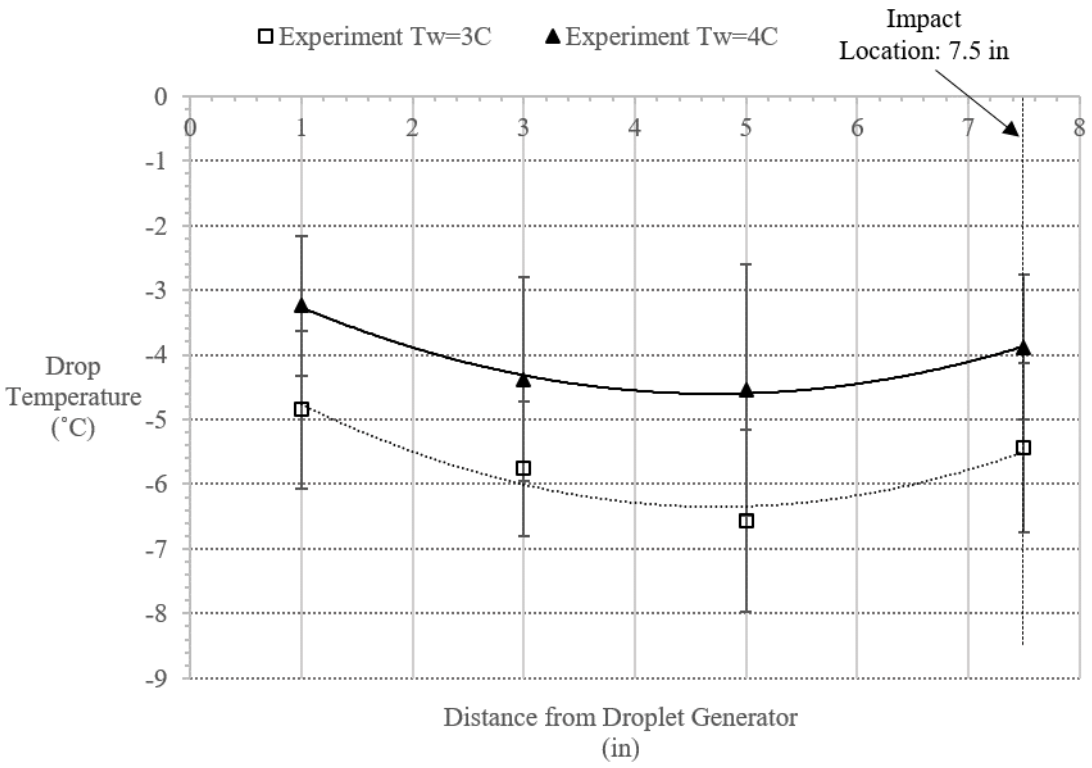

Fig. 10: Droplet temperature versus distance from the droplet generator.

location at the stagnation line of the airfoil model. Instead of only falling 19.05 cm (7.5 in) while in the cold environment, the droplets, using this approach, fell 33.02 cm (13 in). The initial temperature was set to 3 °C since the temperature measured at the droplet generator inlet during the tests was always between 2 and about 4 °C. The vertical velocity used in the simulation was 4 m/s, as the vertical velocity of the droplets analyxed in the chamber ranged between 3 and 4 m/s. The results of the predictions are shown in Figure 11 and indicate that, while the droplet temperature may not be below freezing at the tip (exit of the droplet generator), the water droplet temperature decreases to below 0 °C at the point of impact 33.02 cm (13 inches) below the point of measurement for droplets up to 500 μm in diameter. It should be noted that the droplet generator has a small reservoir where the water collects just above the orifice (Figure 12). While in this small reservoir, the temperature of the water is expected to decrease before it is formed into the stream of droplets that impacts the airfoil model making the approach used to estimate the water supercooling conservative.

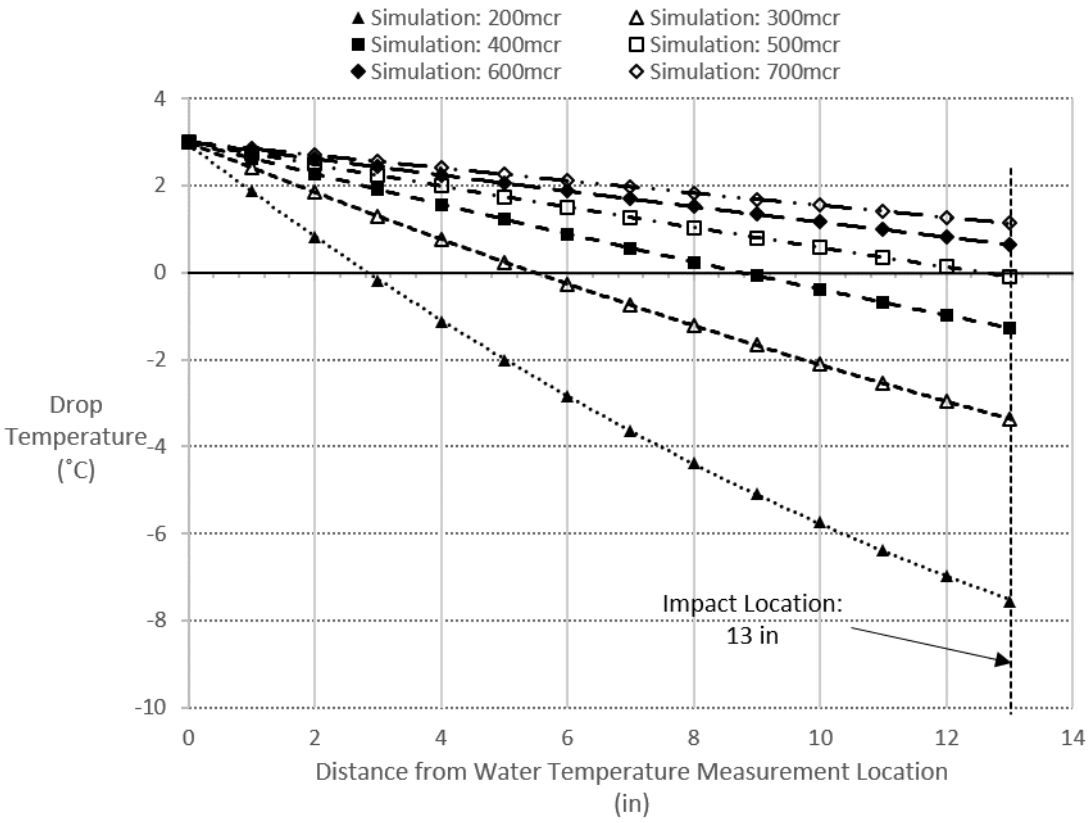

Fig. 11: Droplet temperature versus distance from the droplet generator. Initial Temp = 3 °C.

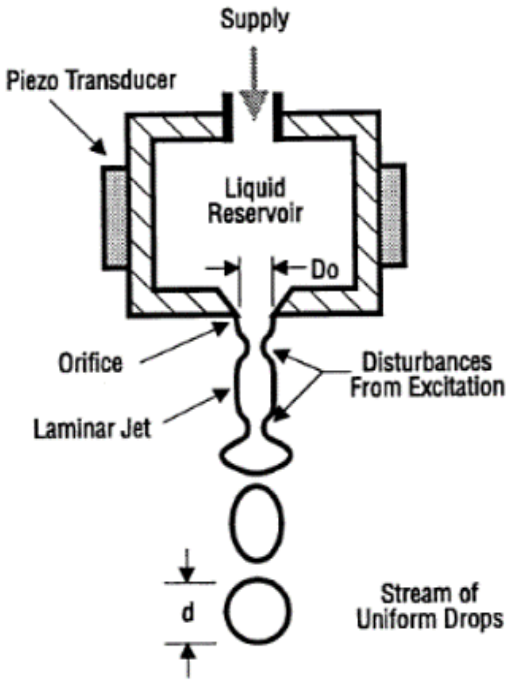

Fig. 12: Schematic of droplet generator showing parts inside of droplet generator [9].

V. Data Analysis

A. Tracking a Single Droplet to obtain the Droplet Displacement against Time

The data analysis is performed using the software program Photron FASTCAM Viewer that allows frame by frame study of the movies, zooming in and out on single frames, running the movies forward and backward, and tracking a single droplet in x-y directions. Using PFV, a high-speed movie corresponding to a set of experimental conditions is opened and the frames where the airfoil impacts the droplets are located. There are multiple sets of frames per movie that show the airfoil passage, because during the test, the camera is programmed to capture images for a certain number of frames. In general, several droplets can be observed impacting the airfoil and, in some cases, breaking up before impact, as shown in Figure 13. For the dropelets shown in Figure 13, the champer temperature was -20 °C and the airfoil velocity was 80 m/s.

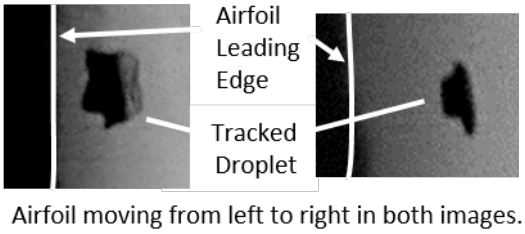

Fig. 13: Droplet breakup before impact. Droplet diameter: Left = 473 μm, Right = 401 μm.

The movie is run backward and forward to study the behavior of the droplets before and during the interaction with the airfoil. A droplet is selected for study and the program is returned to the frame where the airfoil is about to hit the droplet. The droplet may be deforming or is in the process of breaking up. A copy of the frame is saved in the experimental notes and the droplet to be studied is labeled for future identification. The movie is run backward to the frame where there is no indication of deformation or interaction of the droplet with the approaching airfoil and where the tracking is going to be initiated, an example of both frames is shown in Figure 14. The image on the left is the frame where the droplet tracking begins and the last frame used in the droplet tracking is shown in the image on the right. The chamber temperature was -20 °C, the airfoil velocity was 80 m/s, and the diameter of the droplet in the white ovals was initially 473 μm . The frames that contain the motion of the droplet and the interaction with the airfoil are

separated from the larger set of frames to create a shorter video (in Figure 14: 165 frames in video, 1.83 milliseconds in length). This shorter video is saved in .avi file format to be used and processed by the software tracking program.

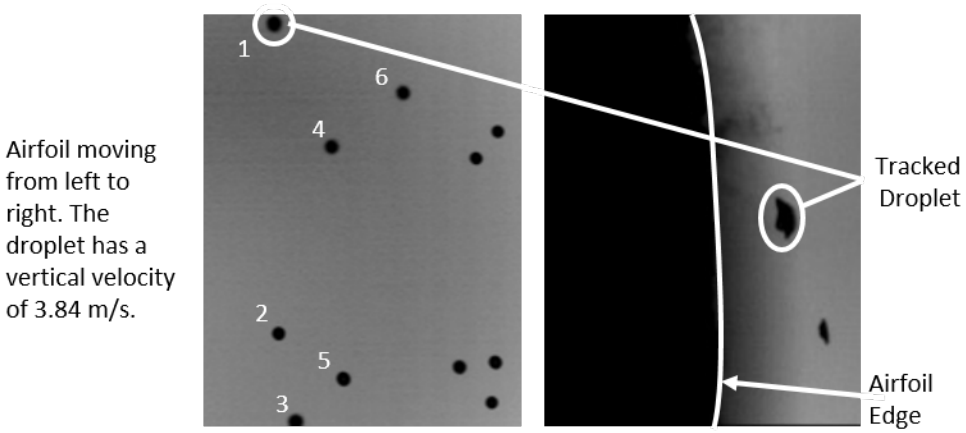

Fig. 14: First and last frame of video of a droplet being tracked with other drops in first frame numbered.

Once the file is in the correct format, it is placed in the proper location. The tracking program requires the frame rate, the number of fames in the video, the droplet number in the first frame (numbering from top to bottom then going left to right, in the case of Figure 14, the droplet to be tracked is droplet number 1 in the frame since it is closest to the left and top edges of the frame), the number of the frame where the airfoil first appears, the airfoil velocity, and the resolution to convert from pixels to micrometers. The program begins by verifying the frame numbers and then calculating the appropriate threshold value to convert the grayscale images to binary images using the Otsu method and prepares the images for the subsequent parts in processing [10]. The program then determines the number of objects in the images and places an ellipse around the droplet being tracked. The centroid of the ellipse is calculated and used to determine the motion of the droplet. From the tracking of the centroid, the motion in pixels relative to the first frame is recorded. For each frame, the following data is recorded and organized in a spreadsheet: the frame number, the time with respect to the first frame in the video, the time with respect to the first frame used to track the droplet, the horizontal displacement of the centroid, the vertical displacement of the centroid, the area of the ellipse, the diameter of the ellipse, the perimeter of the ellipse, and the ellipse major and minor axes lengths. The information is then used to calculate the droplet velocity

and acceleration and the parameters of interest described in the following sections.

B. Calculation of the Horizontal Velocity and Acceleration of the Droplet against Time

A curve fit of the droplet displacement against time is generated and used to calculate the horizontal velocity and acceleration of the droplet. The curve fit is a double five parameter exponential growth equation. The first and second derivatives of the equation give the droplet velocity and acceleration. These are the droplet horizontal velocity and acceleration against time measured by an observer located on a frame of reference at rest with respect to the test cell.

C. Change from the Frame of Reference at the Test Cell to the Frame of Reference at the Airfoil

The horizontal displacement, velocity, and acceleration were initially measured in a frame of reference at rest with respect to the test cell. It is more convenient to work in a frame of reference at rest on the airfoil. The frame of reference located on the airfoil has the origin located at the stagnation point on the leading edge. In a strict sense, a frame of coordinates at rest with respect to the airfoil is not an inertial frame because the airfoil is rotating, it is accelerated. Since the interaction between the droplets and the airfoil occurs at a distance less than or equal to the airfoil chord, that section of the airfoil path is nearly straight and the frame of reference at rest with respect to the airfoil is assumed as inertial during that part of its path. The Galilean transformation together with the airfoil velocity was used to convert the velocity and acceleration of the droplet from the frame of reference at the test cell to the frame of reference at the airfoil (Figure 15, velocity and acceleration of droplet shown in Figure 14).

D. Position of a Droplet with Respect to the Frame of Reference at the Airfoil

At a given location along the droplet path, the number of camera frames separating the droplet from the airfoil is equal to the frame number at which the airfoil hits the droplet minus the frame number at the given location of the droplet. Multiplying the number of frames separating the droplet and the airfoil by the time lapse between frames (1/frame rate) and by the airfoil speed gives the horizontal position of the droplet with respect to the frame of reference at the airfoil. Repeating the

calculation for each droplet location gives the distance of the droplet along its horizontal path with respect to the leading edge of the airfoil. The main parameters in the experiment were calculated at each position of the droplet as it approaches the airfoil and with respect to the frame of reference located at rest on the airfoil.

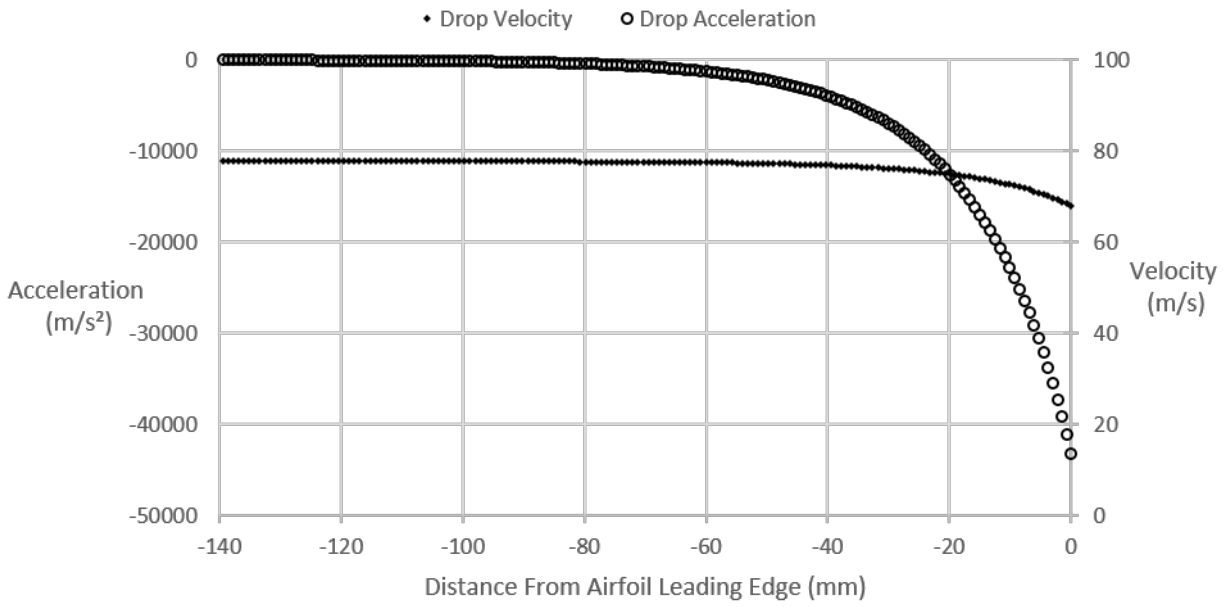

Fig. 15: Droplet horizontal velocity and acceleration in the frame of reference at rest on the airfoil.

E. Air Velocity at a given Droplet Location

For an airfoil with the same geometry as the DBKUP 02 but scaled down 1/10 in size (0.047 m chord), the air velocity along the horizontal line ending at the stagnation point on the leading edge was measured experimentally with a Laser Doppler Velocimeter (LDV) at the INTA 0.3 m x 0.2 m wind tunnel. The wind tunnel results were compared to particle image velocimetry (PIV) measurement results that were obtained using the rotating rig test cell and the results were similar. The experimental data was curve-fit and the resulting equation was used to approximate the air velocity at any given droplet position along its path. The dependent variable is the air velocity divided by the free stream velocity (V_{air}/V_{∞}). The independent variable is the distance with respect to the leading edge of the airfoil divided by the chord (x/c). To calculate the position of the droplet using the curve fit equation the value of the free stream velocity is needed. For the frame of

reference at rest with respect to the airfoil, the air free stream velocity is the same as the velocity of the airfoil with respect to the frame of reference at rest with respect to the test cell. The chord of the airfoil (chord = 0.47 m (18.5 in)) is used to obtain the dimensional distance ahead of the airfoil. Although the equation used to approximate the air velcity was obtained using a correlation of data collected in a wind tunnel, as mentioned earlier, the distance covered by the airfoil as it interacts with the droplets is less than or equal to the airfoil chord and therefore, the path of the airfoil is assumed to be straight in the calculation of the air velocity. Since the experimental setup and the airfoil are similar to those used in the INTA experiments, the same correlation used to determine the air velocity at various distances ahead of the airfoil was used in the analysis of the droplet data obtained in the AERTS facility.

F. Relative Velocity between the Droplet and the Air (Slip Velocity)

Since at each droplet position along its path the horizontal velocity of the droplet and the velocity of the air are known, the relative velocity between the droplet and the air can be calculated. This velocity, $|V_{air}\text{-}V_{droplet}|$, is called the slip velocity. The three velocities, the droplet, air, and slip velocities, for the droplet shown in Figure 14 are shown in Figure 16. The Reynolds number and the Weber number can be calculated when the horizontal slip velocity at each location along the droplet path is known.

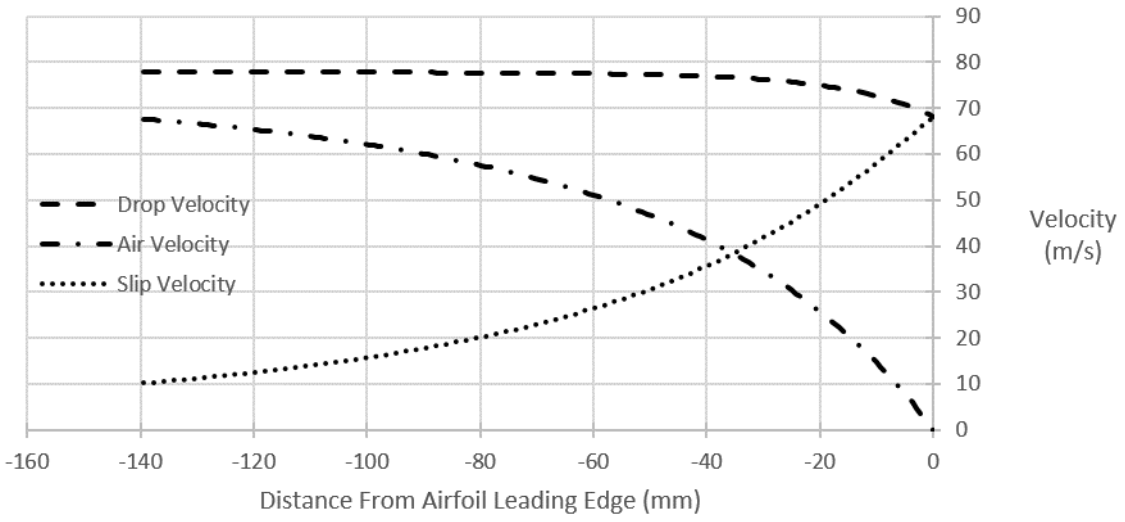

Fig. 16: Droplet, air, and slip velocity against distance from the leading edge of the airfoil.

G. Calculation of the Reynolds Number, the Weber Number, and the Bond Number

The main parameters measured along the path of the droplet were the Reynolds number (Eq. 2), the Weber number (Eq. 3), and the Bond number (Eq. 4). The three parameters were measured with respect to the horizontal motion of the droplet. The droplets leave the monosize droplet generator and fall vertically at a constant speed between 3 and 4 m/s (measured during the experiment). There was no indication from the physical behavior of the droplet that the vertical velocity had an influence on the deformation of the droplet. The shape of the droplet during deformation corresponded to the response of the droplet to the horizontal velocity and acceleration. In all the measurements and calculations, the vertical velocity was not considered.

The following are the definitions of the main parameters measured along the path of the droplet:

Reynolds Number:

$$Re = \frac{\rho_{air}|V_{air} - V_{droplet}|D}{\mu_{air}} \tag{2}$$

Weber Number:

$$We = \frac{\rho_{air}|V_{air} - V_{droplet}|^2 D}{\sigma_{\frac{water}{air}}} \tag{3}$$

Bond Number:

$$Bo = \frac{\rho_{water} D^2}{\sigma_{\frac{water}{air}}} \left(\frac{dV_{droplet}}{dt} \right) \tag{4}$$

where D is the droplet diameter, $V_{droplet}$ is the droplet velocity, V_{air} is the air velocity at the location of the droplet, (V_{air} - $V_{droplet}$) is the slip velocity, ρ_{air} is the air density, μ_{air} is the air absolute viscosity, ρ_{water} is the water density for the droplet, $\sigma_{\frac{water}{air}}$ is the water surface tension for the droplet. The Bond number was defined with respect to the droplet acceleration. The values used while processing the data are the values provided in Tables 2 and 3 for air and water at room temperature (20 °C). The effect of temperature on the values obtained for the Bond number are small. The Bond number of 8 droplets using the fluid properties at room temperature are plotted

Table 2: Values for air density and viscosity at three different temperatures.

Temperature (°C)	Air Density (kg/m^3)	Air Viscosity (μPa s)
20	1.204	18.369
0	1.269	17.362
-20	1.394	16.321

Table 3: Values for water density and surface tension at three different temperatures.

Temperature (°C)	Water Density (kg/m^3)	Surface Tension (N/m)
20	998.2	0.07273
0	999.9	0.07575
-5	999.3	0.07637

along with the Bond number calculated using air properties at -20 °C and water properties at 0 °C in Figure 17. The difference observed in the Bond number is less than 5 %.

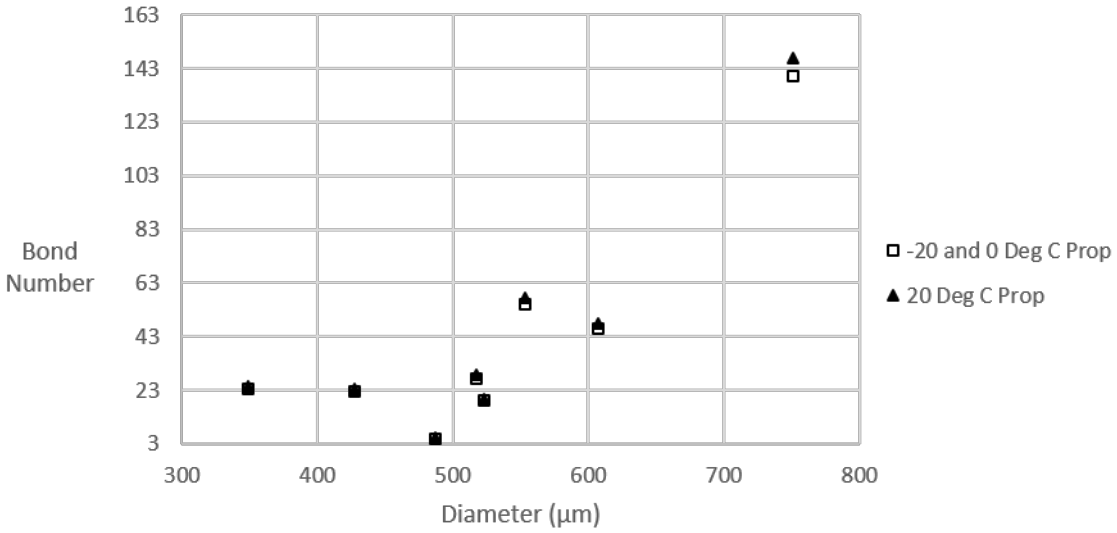

Fig. 17: Bond number against droplet diameter. Initial velocity = 70 m/s, slip velocity = 50 m/s.

Since the air and water droplet properties are known and the droplet diameter, the slip velocity, and the droplet acceleration are calculated along the path of the droplet, then the non-dimensional parameters can be calculated. The velocities and accelerations used in the calculation of the parameters are for the horizontal direction. Considering that the parameters listed above in Equations

2 - 4 are functions of the horizontal velocity and acceleration of the droplet, uncertainties in the calculations are expected. The first and second derivatives are taken of the curve fit to the displacement data of the droplets. Therefore, the velocity and acceleration calculations are expected to include uncertainties that are traced back to any uncertainties due to the particular curve fit equation chosen to represent the displacement.

The parameters are calculated for a quasi-steady flow since evidence for unsteady flow around the droplets was not observed in the images captured in the AERTS facility or at the INTA rotating rig. The droplet velocity is based on the images captured and the air velocity is calculated using a curve fit. The curve fit equation was obtained using experimental data in a similar setup as in the present work. Additionally, the velocity of the flow field ahead of the moving airfoil was measured using PIV at the INTA rotating rig. The results are presented for 50 flow field measurements and the average flow field and a two-dimensional map of the standard deviation related to the measurements of the velocity are shown in Figures 4 and 5 of Reference [2]. The researchers conducting the experimental flow characterization found that the spread in the results increased with velocity and that in the case of an airfoil velocity of 90 m/s, the velocity varied by ± 3 m/s.

VI. Results

A. Comparison of Supercooled Droplet and Room Temperature Droplet Data Collected in the AERTS Facility and in INTA

For the comparison of the droplet behavior, data from the tests done at INTA at room temperature are compared to data from the tests done in the AERTS facility at -20 °C chamber temperature. Although the airfoil speeds for the tests are different, 90 m/s for INTA tests and 80 m/s for the AERTS facility tests, the behavior of the droplets at a slip velocity of 60 m/s is compared. The deformation (ellipse major axis/ellipse minor axis) and the Bond number of the droplets are plotted against the droplet diameter in Figure 18 and Figure 19 respectively. The tests at INTA used droplet generator orifice sizes ranging from 500 to 1000 μm while 200 and 400 μm droplet generator orifice sizes were used when testing in the AERTS facility. The lack of overlap in the data does not allow for proper comparisons to be made between the droplets in relation to their behavior. Yet, both the supercooled droplets and the room temperature droplets behave in a similar manner in

that larger diameter droplets tend to have higher deformation than smaller droplets. This can be observed via visual inspection. Two distinct sets of data related to the warm temperature case and the supercooled case arise in the comparison presented in Figure 18, delimited by the line sketched in the graph.

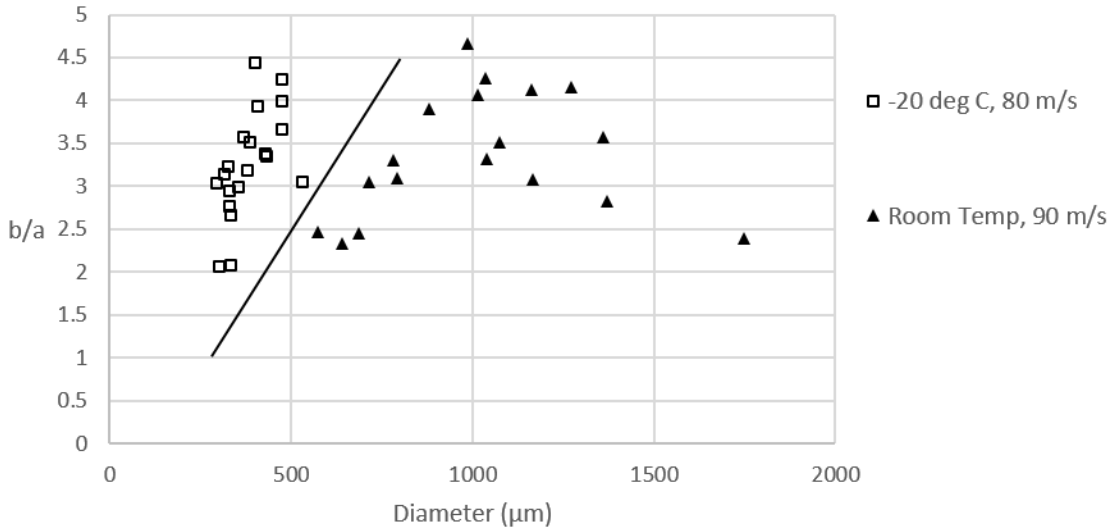

Fig. 18: Droplet deformation against diameter at a slip velocity of 60 m/s.

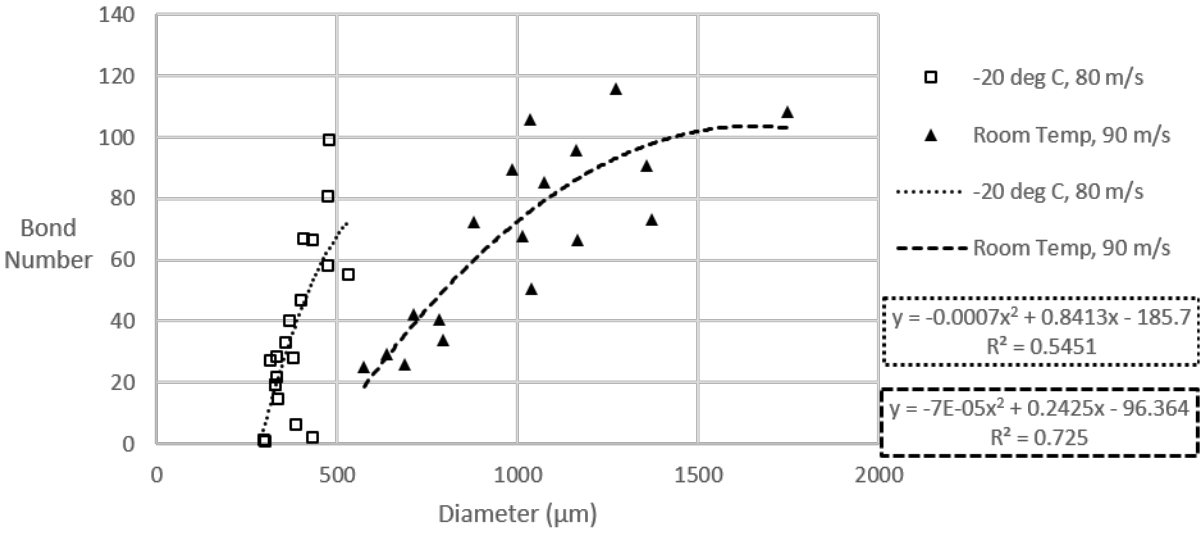

Fig. 19: Bond number against droplet diameter at a slip velocity of 60 m/s.

Given that the described comparisons are conducted at varying airfoil velocities, environmental temperatures, and droplet sizes, a conclusion regarding the effects of droplet supercooling on the

deformation of the drops cannot be made. However, let it be assumed that the supercooling of the droplets has no effect on the droplet fragmentation. If this is the case, the Bond number would not change. Water surface tension is the main parameter in the Bond number that would vary with temperature. The assumption of equal droplet deformation behavior for both environmental conditions assumes that the surface tension of the drops can be estimated to be constant given the small (less than 5%) variation of water surface tension between room temperature and -5 °C water droplets (see Appendix A). If this is the case, the Bond number can be plotted versus droplet size (Figure 19).

The uncertainty in the calculation of the Bond number shown in Figure 19 and in the following Bond number versus droplet diameter graphs is difficult to quantify. Hundreds of frames from multiple repeated tests were studied to find a small number of droplets that were trackable and useful for the present analysis. As explained in Section V Part A, the droplets that were in focus and that were trackable from no deformation to deforation/breakup and impact were chosen for analysis. Many droplets in the videos could not be used because they were not in focus or trackable. For this reason, uncertainty bars and bands are not available for all parameters calculated for the different tests. The differences in the values of the Bond number for droplets of similar size and conditions are noticeable in the graphs shown in this section. The uncertainty bars for the supercooled droplet data presented in Figure 19 is shown below in Figure 20.

Each of the four markers represents the average droplet size of a bin that contains several droplets. The droplets are chosen based on their size, and the maximum percent difference between the droplet diameters within a bin is less than 9%. The uncertainty bars for the droplet diameter are included in the figure. The Bond number corresponding to each marker is the average Bond number of the droplets in the bin. The uncertainty bars for the standard deviation of the Bond number within each bin are also included and the values are listed in Table 4.

A direct comparison to study the effects of temperature cannot be made using the warm droplet results from INTA and the supercooled droplet results from the AERTS facility. Using the experimental setup in the AERTS facility, droplets larger than 500 μm will not be supercooled at the impact location due to the facility temperature limitations. Larger droplets require lower tempera-

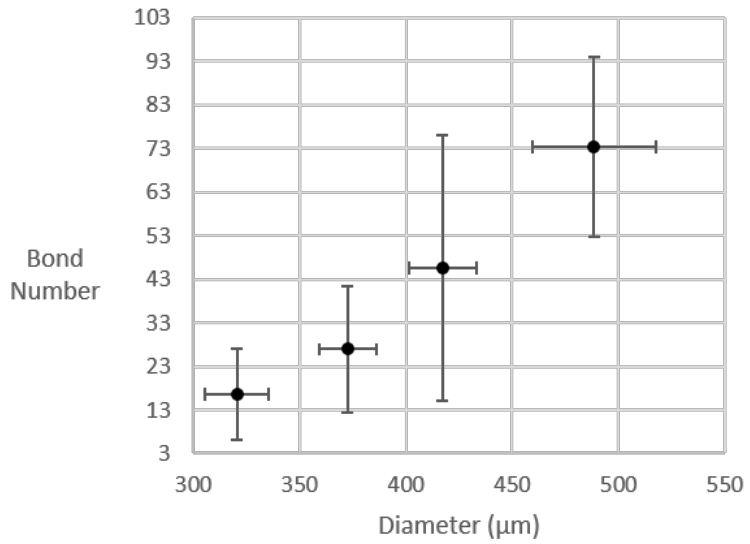

Fig. 20: Bond number against droplet diameter including uncertainty bars.

Table 4: Droplet diameter and Bond number uncertainty values.

Number of Drops	Avg Drop Diam (μm)	Diam Std Dev (μm)	Avg Bo	Bo Std Dev
8	321	15.1	16.6	10.6
4	373	13.5	26.9	14.5
4	417	16	45.6	30.4
4	489	29	73.4	20.7

tures and/or larger residence times to supercool. However, the results suggest that there is a velocity effect between the two sets of data investigated (room temperature vs. supercooled droplets). To further explore the reason for the difference between the two environmental conditions explored, the deformation of droplets at the same temperature for varying airfoil velocities (initial droplet velocity in the fixed frame) are compared in the next section.

B. Effect of Initial Velocity on Deformation and Bond Number

The deformation for the impacting drops tested at varying airfoil velocities plotted against the droplet diameter are shown in Figure 21. For these cases, the air temperature is -20 °C and the slip velocity is 50 m/s. A slip velocity of 50 m/s is used in order to compare multiple higher airfoil velocities. The initial droplet velocities related to the airfoil velocity in the rotating frame are 80 m/s, 70 m/s, and 60 m/s. Such comparison allows for the investigation of the effects of velocity

(initial and slip) on the droplet deformation. In the conducted correlation, trendlines were added to assist with the interpretation of the results. The slopes obtained are in agreement in magnitude, and there is no indication of a particular trend with variations in velocity (see Figure 21).

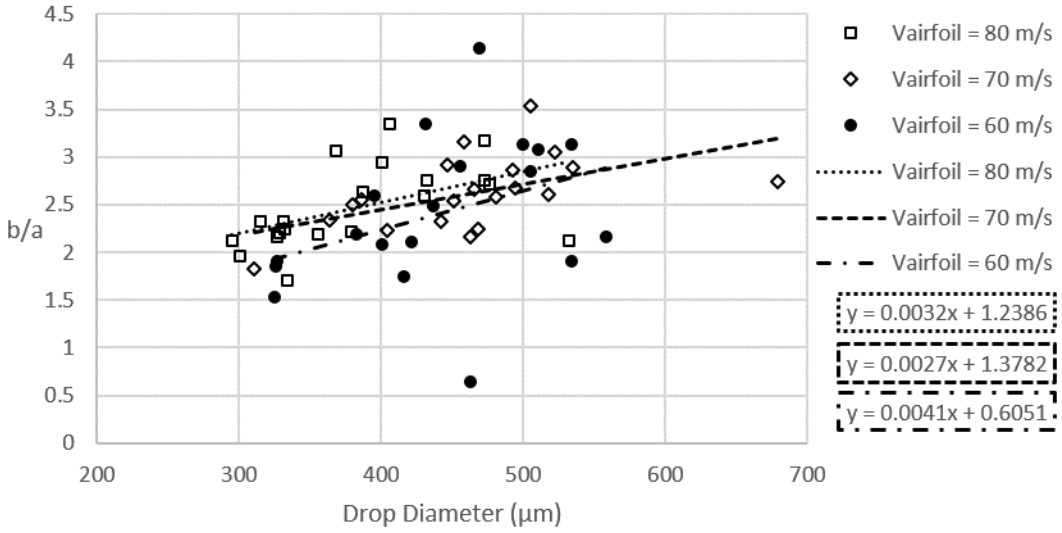

Fig. 21: Droplet deformation against diameter at a slip velocity of 50 m/s and chamber temperature of -20 °C.

To investigate the effects of slip velocity, the deformation against droplet diameter for droplets with initial velocity of 70 m/s and at four slip velocities at a chamber temperature of -20 °C is plotted in Figure 22. For an initial droplet velocity of 70 m/s, the droplet deformation slope at a slip velocity of 30 m/s is 0.0011. As the slip velocity of the drop increases to 60 m/s, the droplet deformation slope increases to 0.0065. These results indicate that the value of the slip velocity relative to the initial velocity affects the slope of the droplet deformation with respect to the droplet size. The results also show that as the slip velocity approaches the initial velocity, the spread in the results increases. Given such variations in the droplet deformation slopes with respect to the droplet size, the initial droplet velocity and the slip velocity must be the same to investigate the effects of supercooling on droplet deformation. The following section compares the deformation of droplets with an initial drop velocity of 60 m/s at a slip velocity of 40 m/s and an initial droplet velocity of 70 m/s at a slip velocity of 50 m/s at two different environmental temperatures in an attempt to determine the effects of water temperature on droplet deformation.

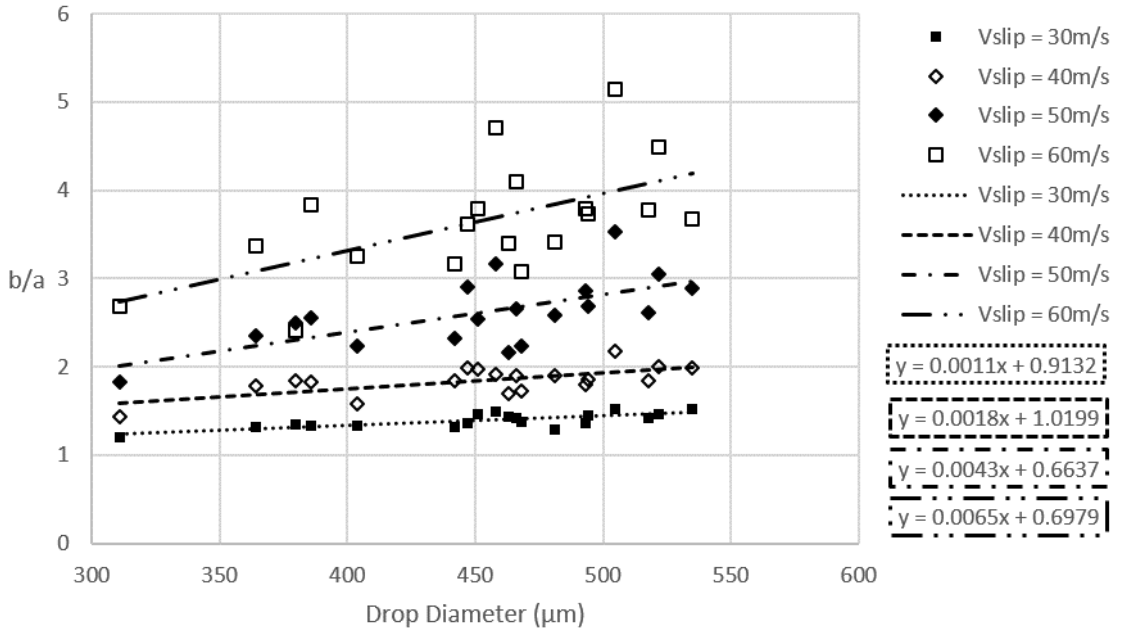

Fig. 22: Deformation against droplet diameter. Initial velocity = 70 m/s, Chamber temperature = -20 °C.

C. Comparison of Supercooled Droplets and Room Temperature Droplet Data Collected in the AERTS Facility

It has been established that to determine the effects of droplet supercooling on its deformation prior to impact with an airfoil, identical slip and droplet initial velocities must be compared. In addition, an effort is made to also compare data containing similar droplet diameters. The data collected using an airfoil speed of 60 m/s in the AERTS facility at 20 °C (room temperature) and -20 °C were used. The droplet deformation at a slip velocity of 40 m/s is plotted below in Figure 23. The data in the figure overlap as all of the droplets analyzed have similar diameters, and trends indicating differences between warm droplets and supercooled droplets is not observed for the tested conditions. Based on these results, it is expected that the Bond number for the two environmental conditions should also agree, suggesting that the variation of the surface tension of the droplets analyzed does not cause a change in the behavior. For this reason, it is assumed that the surface tension of the water is constant for both environmental conditions. If this is the case, it is expected that the Bond number for both temperature cases should follow an equal trend. The bond number for the room temperature case and the supercooled environment is plotted in Figure 24. Both

the warm environment and the supercooled case follow an equal trend. Square polynomial fittings (since Bond number is proportional to the square of the droplet diameter) were added, further showcasing the continuous trends between the results. The processed experimental data suggests that supercooling has no effect on the particle deformation for the airfoil velocity investigated and the droplet temperatures reached.

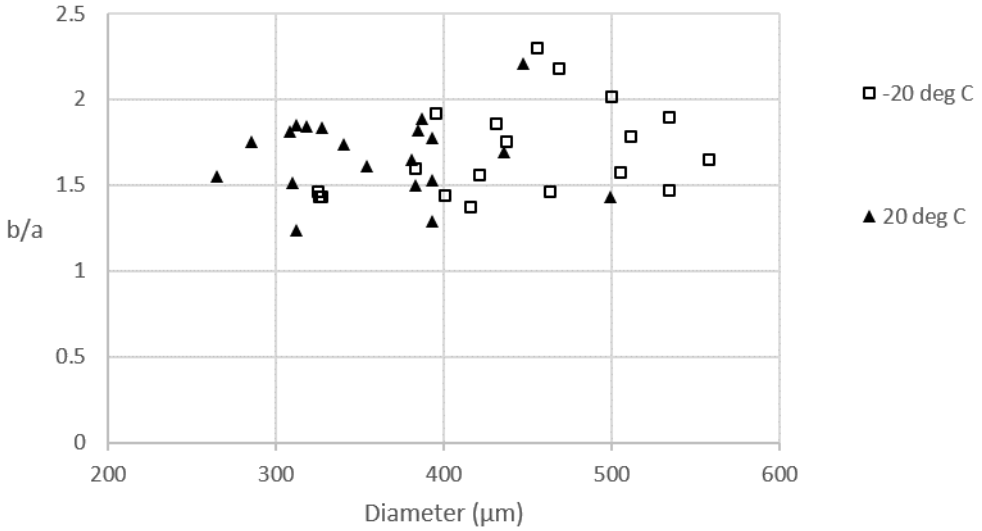

Fig. 23: Droplet deformation against diameter. Slip velocity = 40 m/s, initial velocity = 60 m/s.

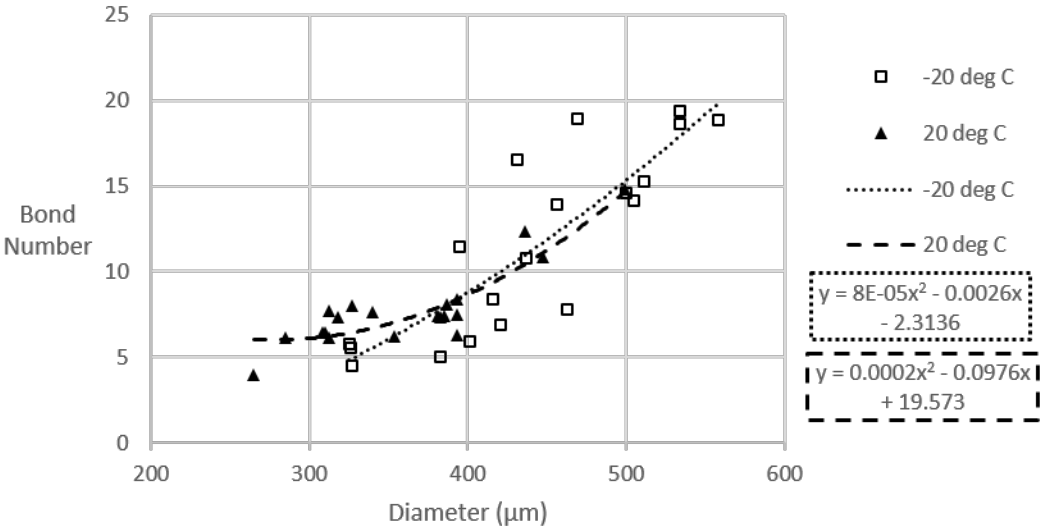

Fig. 24: Bond number against diameter. Slip velocity = 40 m/s, initial velocity = 60 m/s.

Room temperature and supercooled droplets with an initial velocity of 70 m/s and at a slip

velocity of 50 m/s were also compared. The results are shown in Figures 25 and 26. The results also suggest that there is no significant change in behavior due to the changes in temperature obtained during the tests.

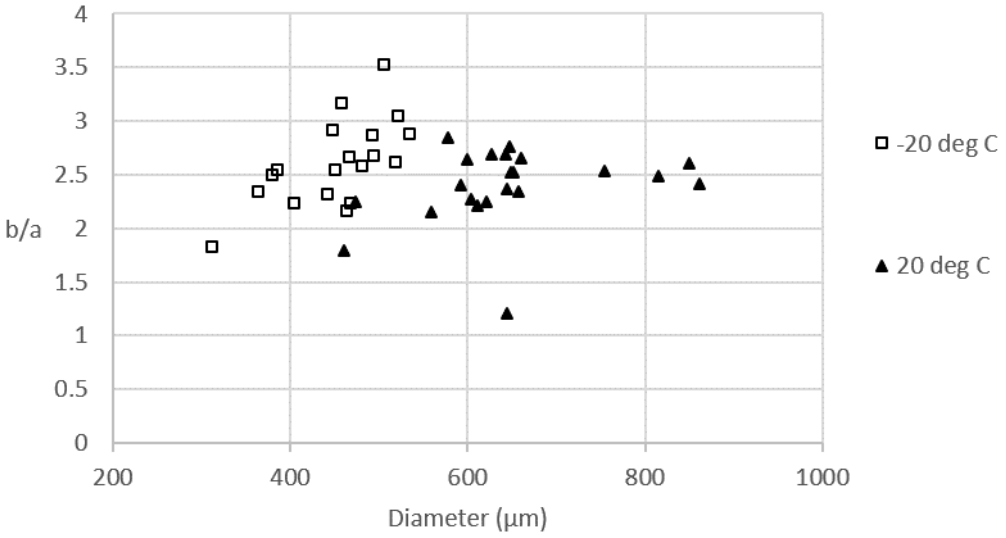

Fig. 25: Droplet deformation against diameter. Slip velocity = 50 m/s, initial velocity = 70 m/s.

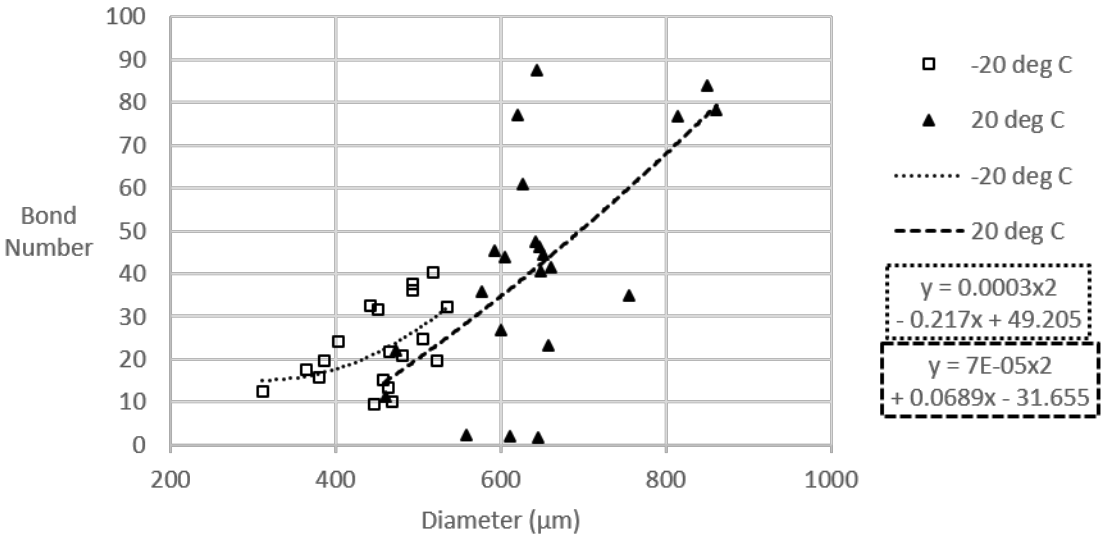

Fig. 26: Bond number against diameter. Slip velocity = 50 m/s, initial velocity = 70 m/s.

VII. Conclusions

The purpose of the work presented here was to determine the effects of supercooling on the behavior of water droplets near the leading edge of an airfoil. The room temperature droplet data that was collected at the Instituto Nacional de Técnica Aeroespacial in Spain was compared to the data collected of supercooled droplets in the Adverse Environment Rotor Test Stand facility. The two sets of data could not be used in the comparison of the behavior as the data did not overlap. Although the same slip velocity was compared, the ranges of droplet diameters and the airfoil velocity were different. It was demonstrated that to compare the effects of water supercooling on droplet deformation, the slip velocity and the initial droplet velocity must be equal.

To explore the effects of the droplet velocity on the deformation of droplets, experimental cases with constant slip velocity and varying airfoil velocity were investigated. A specific trend was not observed in the slopes of the data, but when the airfoil velocity was held constant and the slip velocity was varied, a clear effect on droplet deformation was observed. As the slip velocity approached the airfoil velocity, the slope of the data increased. For an airfoil velocity of 70 m/s and a slip velocity of 30 m/s the slope was 0.0011 and it increased to 0.0065 at a slip velocity of 60 m/s. This indicated that the slip velocity and the airfoil velocity should be the same when comparing data to determine the effects of supercooling on droplet behavior.

A case with equal slip velocity and initial velocity was selected for room temperature and supercooled droplet conditions. The airfoil velocity was 60 m/s and the slip velocity for both sets of data was 40 m/s. Another case with an airfoil velocity of 70 m/s and a slip velocity of 50 m/s was also selected at room temperature and in the supercooled droplet conditions for comparison. In these cases, the deformation of the supercooled droplet and that of the room temperature droplets did not present different trends for the range of weakly supercooled states of water droplets tested. The similar behavior for both environmental conditions indicates that weak supercooling had no effect on particle deformation at the selected impact velocity. The assumption of a constant surface tension value for the mentioned conditions was further supported by the equal trend of the Bond number obtained for supercooled droplets and room temperature ones.

Acknowledgments

The authors would like to thank Mr. Chris Lynch and Mr. Quentin Schwinn for their excellent work with the high-speed imaging system. We would also like to thank all of the AERTS facility research assistants that were involved in the setup of the experiments and collection of data. Your help is very much appreciated.

References

[1] Tan, J., Papadakis, M., and Sampath, M. K., "Computational Study of Large Droplet Breakup in the Vicinity of an Airfoil", DOT/FAA/AR-05/42, Final Report, October 2005.

[2] Sor, S., García-Magariño, A., and Velazquez, A., "Rotating Arm-Based Experimental Study on Droplet Behavior in the Shoulder Region of an Aircraft Aerodynamic Surface", International Journal of Aerospace Engineering, Vol. 2017, October 2017.

[3] Feo, A., Vargas, M. and Sor, S., "Rotating Rig Development for Droplet Deformation/Breakup and Impact Induced by Aerodynamic Surfaces," SAE Paper 2011-38-0087, 2011.

[4] Vargas, M., Sor, S., and Garcia-Magariño, A., "Mechanism of Water Droplet Breakup near the Leading Edge of an Airfoil," 4th AIAA Atmospheric and Space Environments Conference, AIAA, New Orleans, LA, 2012, AIAA 2012-3129.

[5] Lynch, F. T. and Khodadoust, A., "Effects of Ice Accretions on Aircraft Aerodynamics," Progress in Aerospace Sciences 2001; 37:667-767.

[6] Soltis, J., Palacios, J., Eden, T., and Wolfe, D., "Ice Adhesion Mechanisms of Erosion-Resistant Coatings," AIAA Journal, Early Edition, June 19, 2014. doi: 10.2514/1.J053208

[7] Palacios, J., Han, Y., Brouwers, E. W., and Smith, E. C., "Icing Environment Rotor Test Stand Liquid Water Content Measurement Procedures and Ice Shape Correlation," Journal of the American Helicopter Society, Vol. 57, (2), April 2012, pp. 29-40.

[8] Bartkus, T. P., Struk, P. M., Tsao, J. and Van Zante, J. F., "Numerical Analysis of Mixed-Phase Icing Cloud Simulations in the NASA Propulsion Systems Laboratory," 8th AIAA Atmospheric and Space Environments Conference, AIAA, Washington D.C., 2016, AIAA 2016-3739.

[9] TSI Incorporated. (2013) Phase-Doppler Measurement of Known Droplet Size Using the Tsi Mdg-100, Tech. rep.

[10] Otsu, N., "A Threshold Selection Method from Gray-Level Histograms," IEEE Transactions on Systems, Man, and Cybernetics, Vol. 9, No. 1, 1979,pp. 62-66.

[11] Hacker, P. T., "Experimental Values of the Surface Tension of Supercooled Water," NACA TN-2510, October 1951.

APPENDIX A

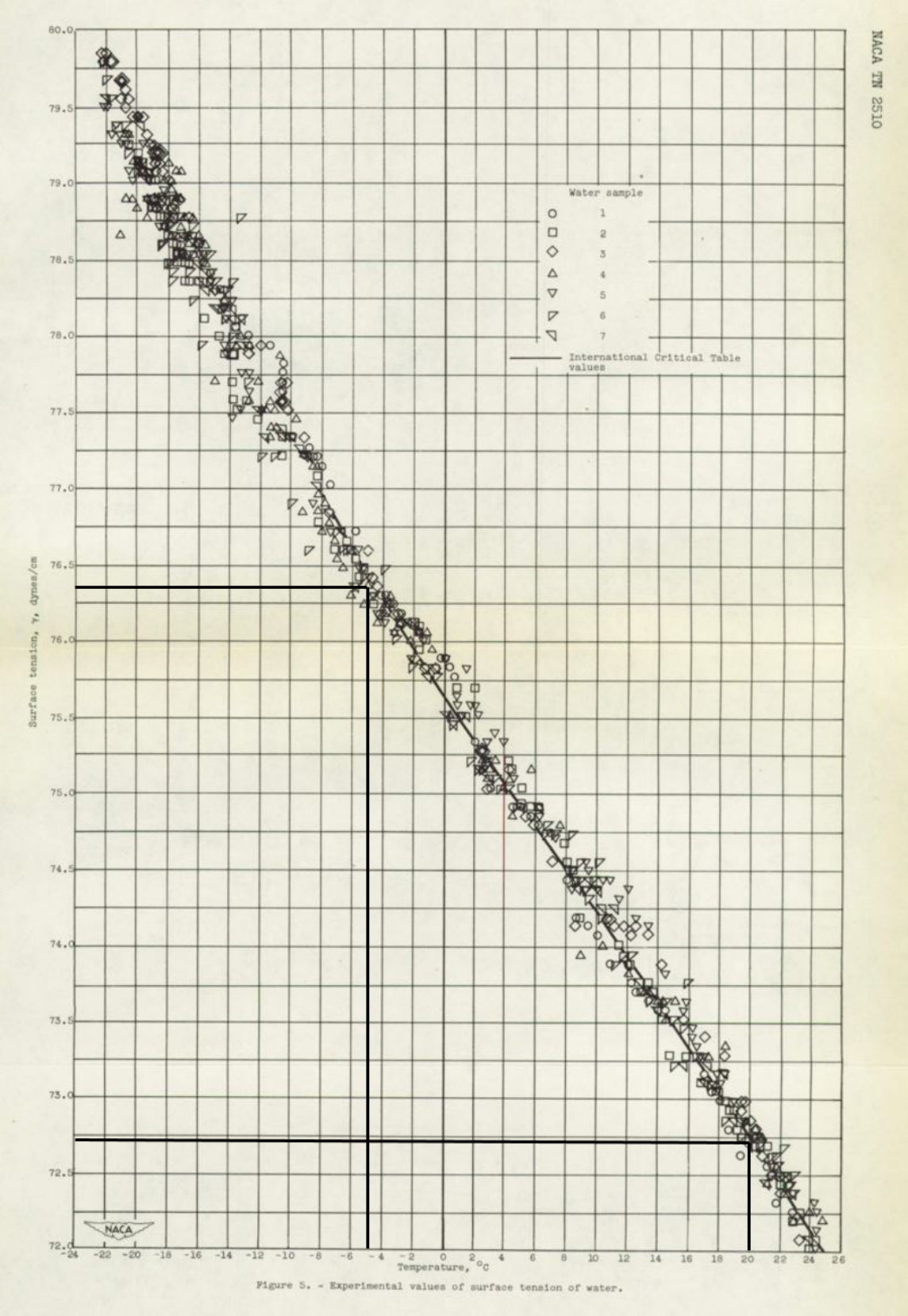

Fig. 27: Experimental water surface tension values versus temperature [11].